IEEE Access
Multidisciplinary | Rapid Review | Open Access Journal

Received December 23, 2020, accepted January 21, 2021, date of publication February 1, 2021, date of current version February 24, 2021.

*Digital Object Identifier 10.1109/ACCESS.2021.3055792*

# A Low Discrepancy Heuristic Evolution ELM and Ground Effect Theory-Based Serial Hybrid Soft Sensor Model of Floating Height in Air Cushion Furnace

**SHUAI HOU[1], JITONG LIU[1], MEIJUAN BAI[1], FUAN HUA[2], XIAOLIN HAN[1], AND WEIWEI LIU[3]**

[1]School of Information and Electrical Engineering, Hebei University of Engineering, Handan 056038, China
[2]State Key Laboratory of Rolling and Automation, Northeastern University, Shenyang 110819, China
[3]School of Mechanical Engineering, Dalian University of Technology, Dalian 116024, China

Corresponding author: Weiwei Liu (liuww@dlut.edu.cn)

This work was supported in part by the National Key Research and Development Program of China (Energy Consumption Analysis and Optimization Control Software for Construction Machinery) under Grant 2020YFB1709903, in part by the National Natural Science Foundation of China under Grant 61973306 and Grant 61802107, in part by the Natural Science Foundation of Hebei Province under Grant E2017402115, in part by the Open Project Foundation of State Key Laboratory of Synthetical Automation for Process Industries under Grant PAL-N201706, in part by the Science and Technology Innovation Fund of Dalian under Grant 2020JJ26GX040, in part by the Fundamental Research Funds for the Central Universities under Grant DUT20JC19, in part by the Iron and Steel Joint Foundation of Hebei Province under Grant E2020402016, in part by the Funding Project of Overseas Returnees from Hebei Province under Grant C201806, and in part by the Handan City Science and Technology Research and Development Projects under Grant 19422101008-27.

**ABSTRACT** In air cushion furnace, the floating height is a key process parameter which greatly affects the quality and production efficiency of high quality mental strips. However, the floating height is hard to be collected in the complex and abominable industry environment. Furthermore, due to the flow field characteristics, some important process variables are difficult to accurately calculate by traditional mechanism modeling methods. In order to accurately predict the floating height, firstly, a low discrepancy heuristic evolution ELM and ground effect theory based serial hybrid soft sensor model is proposed, which constituted by a mechanism model and two data driven models. Secondly, based on the force equilibrium equation and ground effect theory, the mechanism model is constructed, which describes the relationship between the floating height and the process variables including the jet impact angle. Thirdly, a low discrepancy heuristic evolution ELM is proposed as the data driven model to predict the jet impinging angle. In the data driven model, the novel dual mutation strategies collaboration differential evolution is proposed to guarantee the low discrepancy and physical applicability of data driven model. The effectiveness of the proposed method was validated on the self-developed air cushion experiment platform and got desirable experimental results. The research lays an important foundation for the successful implementation of monitoring and control of the strip floating process.

**INDEX TERMS** Air cushion furnace, hybrid model, height prediction, low discrepancy sequence, evolutionary algorithm, ground effect theory.

## I. INTRODUCTION

The high quality mental strips, such as aluminum alloy strip, electronic copper strip and thin silicon steel strip, are extensively used in automobile industry, national defense industry and electric power industry [1]. The high quality mental strips demand higher requirements for surface quality and performance. However, in traditional heat treatment furnace, the surface of strip may be easily scratched and the heating efficiency is low. In air cushion furnace, the metal strip is suspended in the air and the desirable quality and high heating efficiency is guaranteed by this special work mode [2].

In air cushion furnace, the floating height is a key factor which affects the product quality, production efficiency

The associate editor coordinating the review of this manuscript and approving it for publication was Shih-Wei Lin.

and working safety [3]. The reasons are as follows: a) the surface of strip may be scratched when the floating height is abnormal, b) the floating height affects the efficiency of heating and drying, c) the changes of floating height also affect the tension control during the strip production process. Unreasonable control may lead to strip break or equipment damage. However, due to the high temperature and high pressure environment, the values of floating height are hard to be obtained and the cost of data collection process is very expensive and unaffordable for the enterprises.

For the above reasons, some scholars have developed some mechanism modeling methods to predict the floating height. Based on Navier-Stokes equation and continuity equation, Chen *et al.* established the analytic formula of floating height and validated the effectiveness of this analytic formula [4]. Moretti analyzed the mapping relationship between air box pressure and floating height under different lateral deflections of webs [5]. Chang *et al.* validated the effectiveness of different ground effect theories for analyzing aerodynamic characteristics of pressure-pad air bars. The superiority-inferiority and application scopes of different ground effect theories were summarized [6]. Based on the ideal assumptions, Li *et al.* derived the governing equations for the paper web and the air cushion. The pressure distribution of air cushion area and the deformation of paper web were numerically solved by the finite difference method and the Newton-Raphson method [7]. In fact, the jet impinging angle of the airflow is an unneglectable factor for affecting the strip floating height [6]. However, due to the fluid characteristics of airflow, the jet impinging angle is difficult to be described through the mechanism modeling method.

Due to strong learning ability, the data driven model has got desirable achievements in large amounts of industrial fields [8]. For example, a novel back propagation artificial neural network based on the Levenberg-Marquardt theory was proposed to estimate the benzo[a]pyrene content of smoked meats [9]. Yan *et al.* constructed a soft sensor model DAE-NN to estimate the oxygen content of flue gasses, whose parameters are updated by an improved gradient descent method [10]. In the industrial hydrocracking process, Yuan *et al.* developed some data-driven models based on the deep learning networks and verified the feasibility and effectiveness of these models [11]–[13]. The artificial neural network (ANN) based on back propagation has the drawback of computational complexity. In order to overcome this weakness, the extreme learning machine (ELM) algorithm was proposed [14]. ELM is widely applied to solve the soft sensor problem in industrial fields due to the simple structure, fast learning speed and high computational efficiency [15], [16]. However, the input weights and thresholds of hidden layer of ELM are randomly generated, which affects the universal approximation ability of the algorithm. In order to improve the accuracy, Cristiano and Maccio proposed a low discrepancy extreme learning machine (LDELM) where the input weights and thresholds of hidden layer of ELM are generated by low discrepancy sequence [17].

In recent years, the intelligent optimization algorithms are widely used to improve the accuracy of ELM and have got desirable results. For instance, Zhou *et al.* proposed a SDA-GA-ELM model in which the parameters of ELM are optimized by genetic algorithm (GA). The model achieved higher prediction accuracy for the photovoltaic power output [18]. Moreover, Li and Hu optimized the ELM by GA to predict industrial $CO_2$ emissions and achieved good prediction efficiency [19]. However, the GA has the weak globe exploration ability, which may make the search process premature convergence.

Duo to strong global search ability, differential evolution (DE) was used for optimizing the parameters of ELM [20], [21], [22]. Based on the elite guidance mechanism and the collaboration mechanism, Li *et al.* proposed a dual mutation strategies collaboration differential evolution [23]. The elite guidance mechanism provides a clearer direction for individual mutation. And the collaboration mechanism is employed to balance the global exploration and local exploitation of the algorithm. Nevertheless, because the mutation and crossover in DE have the powerful capability of gene alteration, it is difficult to guarantee the low discrepancy characteristic of network parameters of ELM, which may lead to the performance reduction of algorithm. Besides, the physical constrains are not considered, which can reduce the applicability of ELM in industry.

In view of the physical meaning of mechanism model and strong learning ability of data driven model, the hybrid models (HMs) integrating the advantages of two types of models was constructed and widely applied in many fields, such as meteorology [24], membrane technology [25], metal manufacturing industry [26] and petroleum industry [27]. For example, to predict the deformation of an air preheater rotor in thermal power plant boiler, Wang and Liu constructed a Lab-stacked autoencoders (L-SAE) model based on the mass balance equation, domain knowledge and deep learning [28]. In the air cushion furnace, Hou *et al.* proposed a SBEH hybrid model which includes the mechanism model to predict strip floating height and the selective bagging ensemble model to compensate the prediction error of mechanism model [29]. In recent years, Hou *et al.* proposed parallel hybrid floating height prediction model. The mechanism model is used for height prediction and the error compensation model (ECM) is hard to compensate the error between the actual value and the prediction result [30]. In addition, Hou *et al.* developed a novel soft-transition model for the transition state based on data gravitation to achieve the state identification. And the parallel hybrid model was constructed to predict the floating height. In the parallel hybrid model, the mechanism part was derived by combining thick jet theory and the equilibrium equation force. The random forest as the data model compensated the prediction error [31].

The serial hybrid model as one kind of HMs plays an important role in reducing the complexity of mathematical modeling and realizing the soft measurement of intermediate variables. For instance, to predict the gold leaching rate,

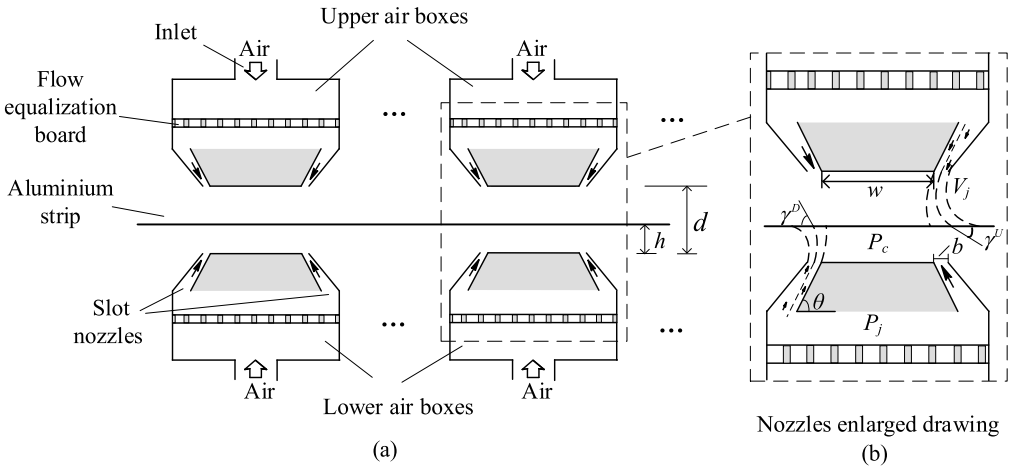


**FIGURE 1.** The structure diagram of air cushion furnace. (a) the main structure of air cushion furnace; (b) The nozzle enlarged drawing.

Zhang *et al.* constructed a serial hybrid model composed of the mass conservation equations and the kernel partial least square, in which the kinetic reaction rates as an intermediate variable is estimated [32]. In the steel refining of the ladle furnace, Lv *et al.* applied the serial hybrid model to real-time predict the sulfur content, and the reaction time as an intermediate variable is predicted by the optimized ELM [33]. In the working process of air cushion furnace, due to the influence of liquid-solid coupling relationships, some important variables are hard to be described by establishing mechanism models. Among them, the jet impinging angle is a key variable for the prediction of floating height and is too difficult to be described by mechanism modeling method. In such cases, the serial hybrid model is suitable for the prediction of the floating height in the air cushion furnace. In addition, there are a lot of noise interference signals in the industrial environment, which deteriorate the precision of the data driven model. Compared with pure data driven model, the serial hybrid model can reduce the impact of the noise samples and the requirement of the amount of training samples. Nevertheless, to the best knowledge of the author, the serial hybrid model has not been found in the air cushion furnace.

In this paper, a serial hybrid soft sensor model is proposed for predicting the strips floating height in air cushion furnace. Firstly, a low discrepancy heuristic evolution ELM and ground effect theory based serial hybrid soft sensor model is proposed to accurately predict the floating height, which is constituted by a mechanism model and two data driven models. Secondly, considering the influence of jet impinging angle $\gamma$, the mechanism model is proposed based on the ground effect theory and force equilibrium equation. Thirdly, the low discrepancy heuristic evolution ELM as the data driven model is presented to predict the jet impinging angle $\gamma$. In the data driven model, a novel dual mutation strategies collaboration differential evolution (NDMCDE) is proposed to guarantee the low discrepancy of parameters and improve the prediction performance of data driven model.

The rest of this paper is organized as follows: the background knowledge of air cushion furnace and the related algorithms are introduced in Section II. The mechanism model of floating height is derived in Section III. Section IV describes the modeling process of data driven model. The serial hybrid soft sensor model is established in Section V. The results of experiments and the analysis are showed in Section VI. The conclusions are given in Section VII.

## II. PRELIMINARIES

In this section, the structure and the workflow of the air cushion furnace are briefly introduced. The basic knowledge of the low discrepancy extreme learning machine and the dual mutation strategy collaboration differential evolution are illustrated.

### A. RELEVANT KNOWLEDGE OF AIR CUSHION FURNACE

Air cushion furnace is an advanced heat treatment equipment for the high-quality metal strips. It can suspend the strip in the air and let the strip do not contact with equipment [29]–[31], so the scratches on the surface of the strip can be avoided in the work process. The structure diagram of air cushion furnace is shown in Figure 1.

As shown in Figure 1, there are $n^U$ upper air boxes and $n^D$ lower air boxes at the top and bottom of air cushion furnace. The distance between upper air box and lower air box is $d$. The upper and lower air boxes are located on the upper and lower sides of the aluminium strip, respectively. Additionally, each air box has two parallel slot nozzles and one inlet. The flow equalization board is installed horizontally inside each air box and can make the air more uniformly distributed. In order to understand the structure more clearly, the nozzles enlarged drawing is shown in Figure 1(b). $w$ is the distance between two slot nozzles. $\theta$ is the jet ejection angle. $b$ is the width of slot nozzles outlet. In the work process, the air enters the air boxes from the inlet and emits from the slot nozzles. Then, the air flows impinge on the upper and lower surface of strip at the velocity of $V_j$.

The jet impinging angle $\gamma^D$ and $\gamma^U$ are generated between the jet centerline of slot nozzles and the strip. Meanwhile, the cushion pressure $P_c$ is also generated between the strip and the air boxes. The lift force is formed and act on the lower and upper surface of the strip, respectively. If the difference of the lift force on the lower surface minus the lift force on the upper surface is equal to the strip gravity, the strip will floats in air cushion furnace. By adjusting the pressure $P_j$ of air boxes, the strip floating height $h$ is controlled within a reasonable range, thus the efficiency of air cushion furnace and the surface quality of product can be guaranteed.

### B. LOW DISCREPANCY EXTREME LEARNING MACHINE

Low discrepancy sequences (LDSs), is a points distribution sequence [34], also known as quasi random sequences (QRSs) [35]. The LDSs, such as the Halton, the Sobol and the Niederreiter, are gradually used in graphics rendering. Figure 2 shows the spatial distribution of 512 samples in 2-D unit cube obtained separately from a Halton LDSs and a pure random sequence. It can be clearly seen that the Halton LDSs sampling (Figure 2(a)) covers the space more evenly than random sequence (Figure 2(b)).

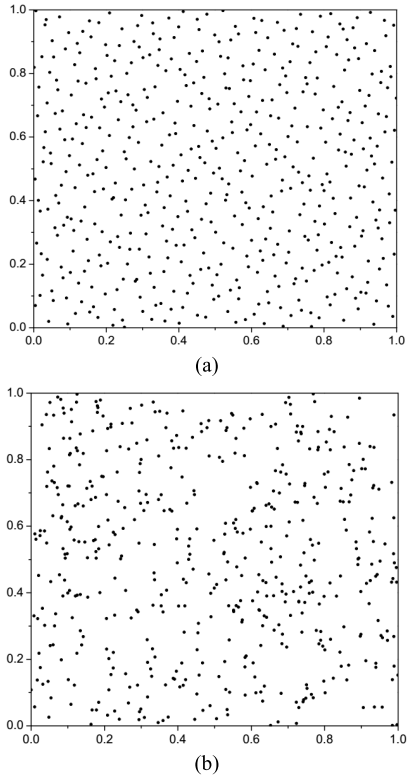


**FIGURE 2.** The spatial distribution of samples in 2-D unit cube: (a) halton LDSs, (b) random sequence.

Different from the traditional ELM, the weights and bias of the hidden layer in low discrepancy extreme learning machine (LDELM) are assigned by LDSs method. It has been proved that the LDELM has better prediction accuracy than ELM [17]. For sample set $\{\boldsymbol{O}, \boldsymbol{T}\}$, where $\boldsymbol{O} = [\boldsymbol{o}_1, \boldsymbol{o}_2, \ldots, \boldsymbol{o}_K]^T$ and $\boldsymbol{T} = [t_1, t_2, \ldots, t_K]^T$. The output of LDELM with $N$ hidden nodes can be represented by

$$f(o_k) = \sum_{n=1}^{N} \beta_n G(\boldsymbol{a}_n, b_n, \boldsymbol{o}_k) = t_k \quad k = 1, \cdots, K \tag{1}$$

where, $\boldsymbol{o}_k = [o_{1,k}, o_{2,k}, \ldots, o_{d,k}]^T$ is the $k$th sample. $\boldsymbol{a}_n = [a_{1,n}, a_{2,n}, \ldots, a_{d,n}]^T$ denotes the weight column vector connecting the $n$th hidden node and input layer. $b_n$ is bias of the $n$th hidden node. $G(^*)$ represents the activation function. $\beta_n$ is output weight of the $n$th hidden node. $d$ is the number of features or dimensions of sample. $K$ is the number of samples.

Discrepancy is an indicator to measure the uniformity of spatial distribution of point set. However, traditional formula of discrepancy has weaker description ability in high dimension space. In this paper, the discrepancy of the network parameters is measured by modified $L_2$-norm method [36]. The calculation formula of discrepancy is shown as follow.

$$M_{2,N}(S)^2 = \left(\frac{4}{3}\right)^D - \frac{2^{1-D}}{N} \sum_{n=1}^{N} \prod_{m=1}^{D} \left(3 - S_{n,m}^2\right) + \frac{1}{N^2} \sum_{n=1}^{N} \sum_{j=1}^{N} \prod_{m=1}^{D} \left[2 - \max\left(S_{n,m}, S_{j,m}\right)\right] \tag{2}$$

where $S = [S_1, S_2, \ldots, S_N]^T$ is a point set in $D$ dimension space, which generated by the Halton. $S_n = (\boldsymbol{a}_n, b_n)$ is the $n$th point in $S$. $N$ is the number of points in $S$. $D = d + 1$ is the number of dimensions. $S_{n,m}$ represents the value of the $m$th dimension of the $n$th point in $S$, $S_{n,m} \in [0, 1]$.

### C. DUAL MUTATION STRATEGY COLLABORATION DIFFERENTIAL EVOLUTION

Differential evolution (DE) was developed by Storn and Price [37]. In the DE, the selection of mutation strategy and evolutionary parameters has a greater impact on performance of algorithm. Thus, Li *et al.* introduced a dual mutation strategy collaboration differential evolution (DMCDE) to obtain the balance between global exploration and local exploitation [23]. The DMCDE mainly includes three parts: 1) mutation, 2) crossover and 3) selection.

#### 1) MUTATION

The mutation strategy DE/e-rand/2 and DE/e-best/2 are presented by introducing the elite guidance mechanism and shown in Equation (3).

$$M_{i,g+1} = \begin{cases} C_{r1,g}^{SP_g} + F_{i,g}(C_{r2,g}^{SP_g} - C_{r3,g}^{IP_g}) \\ +F_{i,g}(C_{r4,g}^{SP_g} 1 - C_{r5,g}^{IP_g}) \\ \qquad\qquad if\ rand(0,1) \le GP_g \\ C_{best,g} + F_{i,g}(C_{r2,g}^{SP_g} - C_{r3,g}^{IP_g}) \\ +F_{i,g}(C_{r4,g}^{SP_g} - C_{r5,g}^{IP_g}) \\ \qquad\qquad else \end{cases} \tag{3}$$

$$GP_g = \frac{1}{1 + e^{1-(G/g)^2}} \tag{4}$$

where $g$ is the index of current generation. $F_{i,g} \in [0, 1]$ is scale factor of $i$th individual in $g$th generation. $NPOP$ is the size of population. The indices $r1$, $r2$, $r3$, $r4$ and $r5$ are mutually exclusive integers randomly generated within [1, $NPOP$]. $rand(0,1)$ obeys a uniform distribution and generates random number within [0, 1]. $G$ is the number of maximum generation. $GP_g$ is the selection probability of DE/e-rand/2 and DE/e-best/2 in $g$th generation. The superior population ($SP_g$) and inferior population ($IP_g$) are formed by dividing the $g$th population $POP_g = [C_{1,g}, C_{2,g}, \ldots, C_{NPOP,g}]$ based on the fitness of individuals. The $C^{SPg}$ is selected from $SP_g$ and the $C^{IPg}$ is selected from $IP_g$. $C_{best,g}$ is the best individual in $g$th generation.

### 2) CROSSOVER

The trial individual $U_{i,g+1}$ is created by carrying out binomial crossover operation on the parent individual $C_{i,g}$ and mutation individual $M_{i,g+1}$ in Equation (5) [38].

$$U^j_{i,g+1} = \begin{cases} M^j_{i,g+1} & if\ rand(0,1) \le CR_{i,g}\ or \\ & j = j_{rand} (j_{rand} \in [1, ND]) \\ C^j_{i,g} & else \end{cases} \tag{5}$$

where $CR_{i,g}$ is the crossover rate of $i$th individual in $g$th generation within [0, 1]. $j_{rand}$ is a integer and randomly chosen from [1, $ND$]. $ND$ is the number of genes in chromosome. $j = 1, 2, \cdots, ND$.

### 3) SELECTION

If the $U_{i,g+}1$ is better than $C_{i,g}$, the $U_{i,g+}1$ will replace the $C_{i,g}$ to enter the next generation $POP_{g+}1 = [C_1, g+1, C_2, g+1, \ldots, C_{NPOP,g+1}]$, and the $NES_i = 0$ is set; else, the $C_{i,g}$ is remained and the $NES_i = NES_i + 1$ is set. Meanwhile, the $F_{i,g+1}$ and the $CR_{i,g+1}$ are updated by Equation (7) and (8)

$$C_{i,g+1} = \begin{cases} U_{i,g+1} & if\ f(U_{i,g+1}) \le f(C_{i,g}) \\ C_{i,g} & else \end{cases} \tag{6}$$

$$F_{i,g+1} = \begin{cases} F_{upper} + rand(0,1) & \\ (F_{upper} - F_{lower}) & if\ NES_i \ge MNES \\ F_{i,g} & else \end{cases} \tag{7}$$

$$CR_{i,g+1} = \begin{cases} CR_{lower} + rand(0,1) & if\ NES_i \ge MNES \\ (CR_{upper} - CR_{lower}) & \\ CR_{i,g} & else \end{cases} \tag{8}$$

where $f(*)$ is the fitness function. $NES_i$ is a counter to record the number of evolution stagnation of $C_{i,g}$. $MNES$ is the maximum number of evolution stagnation. $F_{upper} = 0.5$ and $F_{lower} = 0.1$ are the upper bound and lower bound of $F_{i,g}$, respectively. $CR_{upper} = 0.5$ and $CR_{lower} = 0.1$ are the upper bound and lower bound of $CR_{i,g}$, respectively.

## III. CONSTRUCTION OF MECHANISM MODEL

The mechanism model is derived based on ground effect theory and force equilibrium equation. Considering the influence

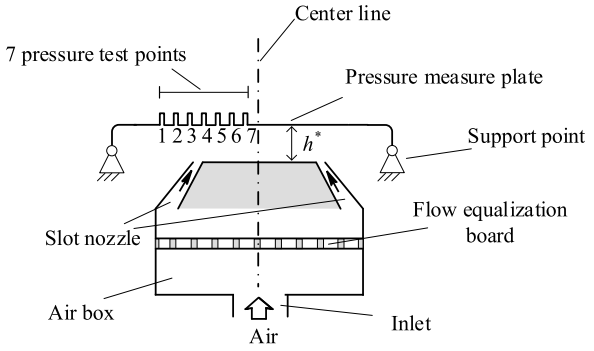


**FIGURE 3.** The schematic diagram of pressure test device.

of jet impinging angle on the floating height, the equation of pressure ratio given by Bradbury is

$$\frac{P_c}{P_j} = \frac{2(\cos\theta + \cos\gamma)}{\frac{h}{b} + \frac{1}{2}\cos\theta + \cos\gamma} \tag{9}$$

where $P_j$ is the pressure of air boxes. $\gamma$ is jet impinging angle between extended jet centerline and horizontal plane of strip. $P_c$ is the cushion pressure. $\theta$ is the jet ejection angle. $h$ is the floating height of strip. $b$ is the width of slot nozzle. The horizontal force balance of the air jet requires

$$\rho b V_j^2 = \frac{P_c h}{1 + \cos\theta} \tag{10}$$

where $\rho$ is the air density and $V_j$ is the jet velocity of the air. The lift force per unit length of air bar is obtained by

$$F = P_c w + 2\rho b V_j^2 \sin\theta \tag{11}$$

where $w$ is the distance between two slot nozzles. By eliminating $P_c$ and $\rho b V_j^2$ from (11) using (9) and (10), we can obtain

$$F = \left(w + \frac{2h\sin\theta}{1+\cos\theta}\right)\left(\frac{2(\cos\theta+\cos\gamma)}{\frac{h}{b}+\frac{1}{2}\cos\theta+\cos\gamma}\right)P_j \tag{12}$$

The pressure of the lower air boxes and the upper air boxes are denoted by $P_j^D$ and $P_j^U$, respectively. The jet impinging angle on the lower surface of the strip is set as $\gamma^D$, and the jet impinging angle on the upper surface is set as $\gamma^U$. Finally, the lift force on the lower surface of strip $F^U$ and lift force on the upper surface $F^D$ is calculated as follows:

$$F^U = \left(w + \frac{2h\sin\theta}{1+\cos\theta}\right) \times \left(\frac{2\left(\cos\theta+\cos\gamma^D\right)}{\frac{h}{b}+\frac{1}{2}\cos\theta+\cos\gamma^D}\right) n^D P_j^D \tag{13}$$

$$F^D = \left(w + \frac{2(d-h)\sin\theta}{1+\cos\theta}\right) \times \left(\frac{2\left(\cos\theta+\cos\gamma^U\right)}{\frac{d-h}{b}+\frac{1}{2}\cos\theta+\cos\gamma^U}\right) n^U P_j^U \tag{14}$$

where $d$ is the distance between the upper air boxes and lower air boxes. $n^U$ and $n^D$ represent the number of the upper and the lower air boxes in the air cushion furnace, respectively.

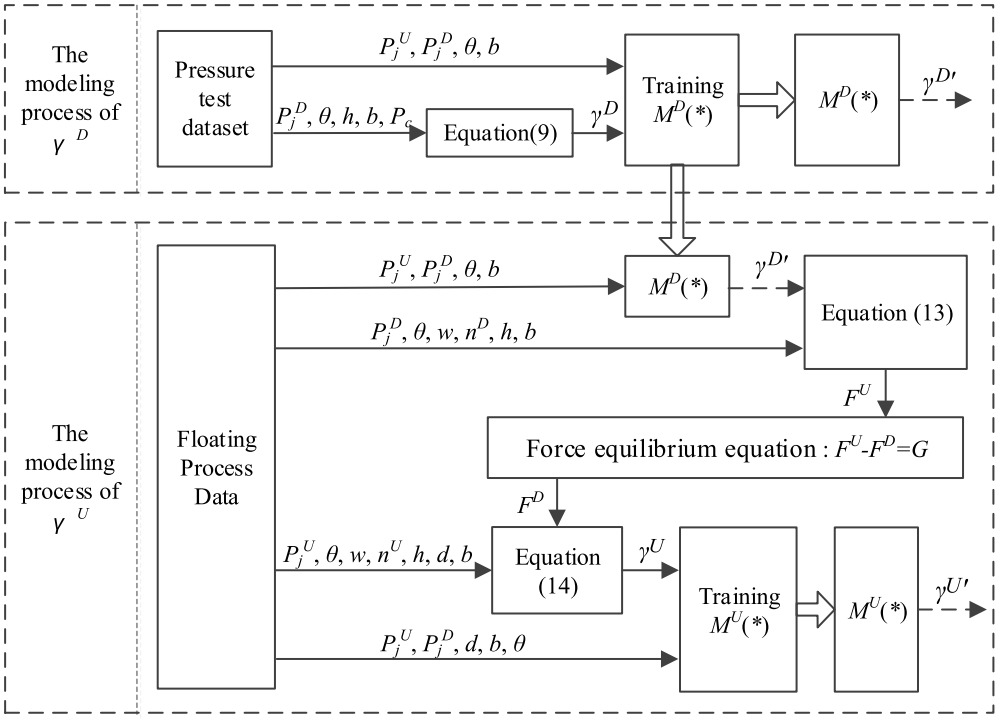


**FIGURE 4.** The modeling process of $\gamma^D$ and $\gamma^U$. (the solid arrows indicate the variables of input and output. The hollow arrows indicate the trained data driven model. The dotted arrows represent the output of the data driven model.)

If the difference of lift force $F^U$ minus lift force $F^D$ is equal to gravity $G$ of strip, the strip will suspend in the air. Based on the force equilibrium equation, the force on the strip can be expressed as

$$F^U - F^D = G \tag{15}$$

By combining Equation (13), (14) and (15), the mechanism formula of floating height can be obtained and shown in Equation (16).

$$\begin{aligned} &Ah^2 + Bh^2\cos\gamma^U + Ch^2\cos\gamma^D + Dh \\ &+Eh\cos\gamma^U + Fh\cos\gamma^D + Hh\cos\gamma^U\cos\gamma^D \\ &+I\cos\gamma^U\cos\gamma^D + J\cos\gamma^U + K\cos\gamma^D + L = 0 \end{aligned} \tag{16}$$

The strip floating height $h$ is calculated by solving Equation (16). In addition, the coefficient $A$, $B$, $C$, $D$, $E$, $F$, $H$, $I$, $J$, $K$ and $L$ in Equation (16) are shown in Equation (17-27).

$$\begin{aligned} A &= 16b\sin\theta\cos\theta\left(n^U P_j^U - n^D P_j^D\right) \\ &\quad +4\left(1+\cos\theta\right)G \end{aligned} \tag{17}$$

$$B = 16b\sin\theta n^U P_j^U \tag{18}$$

$$C = -16b\sin\theta n^D P_j^D \tag{19}$$

$$\begin{aligned} D &= \left[8b^2\sin\theta\cos^2\theta - 8wb\cos\theta\left(1+\cos\theta\right)\right] \\ &\quad \left(n^D P_j^D + n^U P_j^U\right) + 16db\sin\theta\cos\theta \\ &\quad \left(n^D P_j^D - n^U P_j^U\right) - 4d\left(1+\cos\theta\right)G \end{aligned} \tag{20}$$

$$\begin{aligned} E &= 8b^2\sin\theta\cos\theta\left(2n^D P_j^D + n^U P_j^U\right) \\ &\quad -8wb\left(1+\cos\theta\right)n^U P_j^U - 16db\sin\theta n^U P_j^U \\ &\quad -4b\left(1+\cos\theta\right)G \end{aligned} \tag{21}$$

$$\begin{aligned} F &= 8b^2\sin\theta\cos\theta\left(2n^U P_j^U + n^D P_j^D\right) \\ &\quad -8wb\left(1+\cos\theta\right)n^D P_j^D + 16db\sin\theta n^D P_j^D \\ &\quad +4b\left(1+\cos\theta\right)G \end{aligned} \tag{22}$$

$$H = 16b^2\sin\theta\left(n^D P_j^D + n^U P_j^U\right) \tag{23}$$

$$\begin{aligned} I &= 8wb^2\left(1+\cos\theta\right)\left(n^D P_j^D - n^U P_j^U\right) \\ &\quad -16db^2\sin\theta n^U P_j^U - 4b^2\left(1+\cos\theta\right)G \end{aligned} \tag{24}$$

$$\begin{aligned} J &= 4wb^2\cos\theta\left(1+\cos\theta\right)\left(2n^D P_j^D - n^U P_j^U\right) \\ &\quad -8db^2\sin\theta\cos\theta n^U P_j^U \\ &\quad -2b^2\cos\theta\left(1+\cos\theta\right)G \end{aligned} \tag{25}$$

$$\begin{aligned} K &= 4wb^2\cos\theta\left(1+\cos\theta\right)\left(n^D P_j^D - 2n^U P_j^U\right) \\ &\quad +8wdb\left(1+\cos\theta\right)n^D P_j^D \\ &\quad -16db^2\sin\theta\cos\theta n^U P_j^U \\ &\quad -\left(4db + 2b^2\cos\theta\right)\left(1+\cos\theta\right)G \end{aligned} \tag{26}$$

$$\begin{aligned} L &= 4wb^2\cos^2\theta\left(1+\cos\theta\right)\left(n^D P_j^D - n^U P_j^U\right) \\ &\quad +8wdb\cos\theta\left(1+\cos\theta\right)n^D P_j^D \\ &\quad -8db^2\sin\theta\cos^2\theta n^U P_j^U \\ &\quad -b\cos\theta\left(2d + b\cos\theta\right)\left(1+\cos\theta\right)G \end{aligned} \tag{27}$$

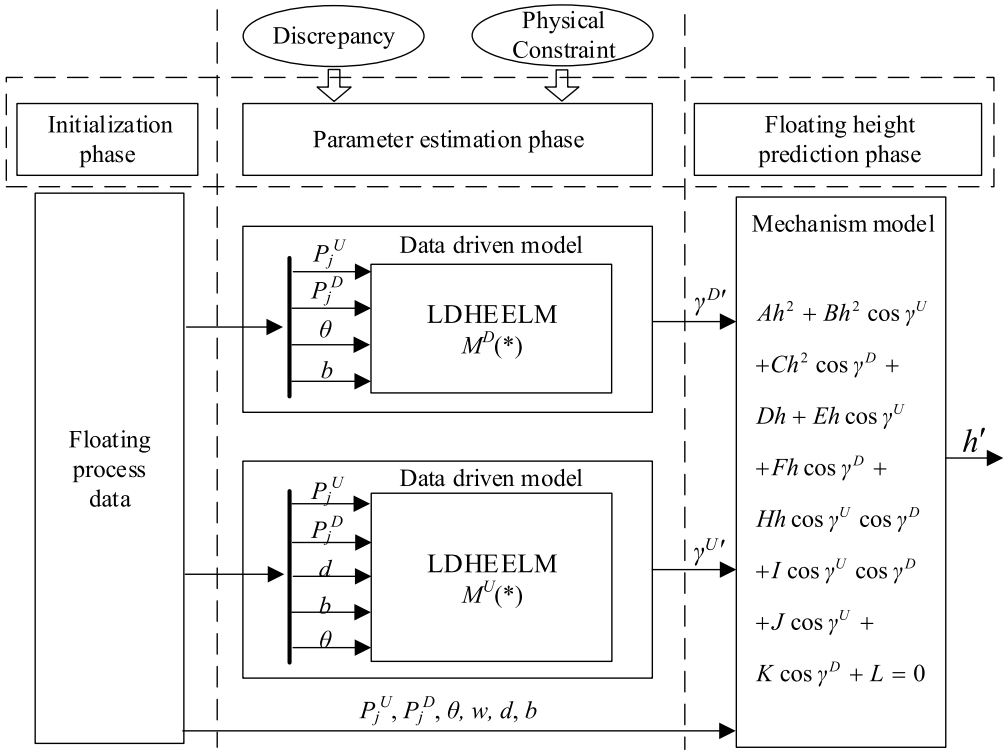


**FIGURE 5.** The framework of serial hybrid soft sensor model.

It can be seen from Equation (16) that the calculation precision of mechanism formula is affected by the $\gamma^D$ and $\gamma^U$. So it is very important to accurately predict the jet impinging angle $\gamma^D$ and $\gamma^U$.

## IV. CONSTRUCTION OF DATA DRIVEN MODEL FOR $\gamma^D$ AND $\gamma^U$

### A. ACQUISITION OF PRESSURE TEST DATASET

In order to obtain pressure test dataset, a pressure test device has been developed and the experiments are carried out on this device. The schematic diagram of pressure test device is shown in Figure 3.

In Figure 3, the pressure test device is mainly composed of a single lower air box and a pressure measure plate. The lower air box is composed of the slot nozzles, inlet and flow equalization board. The flow equalization board is installed inside the lower air box and can make the air more evenly

distributed. The pressure measure plate is placed above the lower air box. The 7 pressure test points are placed on the left side of the pressure measure plate.

The center line of the pressure measure plate coincides with the center line of the lower air box. The geometry size of the lower air box and the pressure measure plate are symmetrically distributed along center line so that pressure distribution on the lower surface of pressure measure plate is mirror-image symmetrical along center line. The height $h^*$ is the distance between the lower surface of pressure measure plate and the upper surface of lower air box, which can be changed by adjusting support points along vertical direction. The height $h^*$ corresponds to the strip floating height $h$. Based on the pressure test device, the experiments are implemented and the values of cushion pressure can be obtained under the different pressure of lower air box and height $h^*$.

### B. MODELING PROCESS OF $\gamma^D$ AND $\gamma^U$

In fact, a strong coupling relationship is existed between $\gamma^D$ and $\gamma^U$ in air cushion furnace. If information of the coupling relationship is not reflected in the dataset, the accuracy of the prediction model will be deteriorated. In order to let the samples in dataset contain the coupling information, the following experimental procedures are carried out and it can be seen in Figure 4.

In Figure 4, the prediction model of $\gamma^D$ is represented by $M^D(*)$ and the prediction model of $\gamma^U$ is represented by $M^U(*)$. The $M^D(*)$ and $M^U(*)$ are constructed based on ground effect theory, lift force formula and force equilibrium equation.

The modeling process of $M^D(*)$ is as follows. First, by bringing the variables $P_j^D$, $\theta$, $h$, $b$ and $P_c$ from pressure test dataset into Equation (9), the jet impinging angle $\gamma^D$ is calculated. Then, the variables $P_j^U$, $P_j^D$, $\theta$, $b$ as the input variables and the $\gamma^D$ as the target variable are selected to train the model $M^D(*)$. Finally, the estimated value $\gamma^{D'}$ can be obtained by the built prediction model $M^D(*)$.

The modeling process of $M^U(*)$ is as follows. According to the built $M^D(*)$, the $\gamma^{D'}$ is estimated by using the variables $P_j^U$, $P_j^D$, $\theta$ and $b$ from floating process dataset. Then, the lift

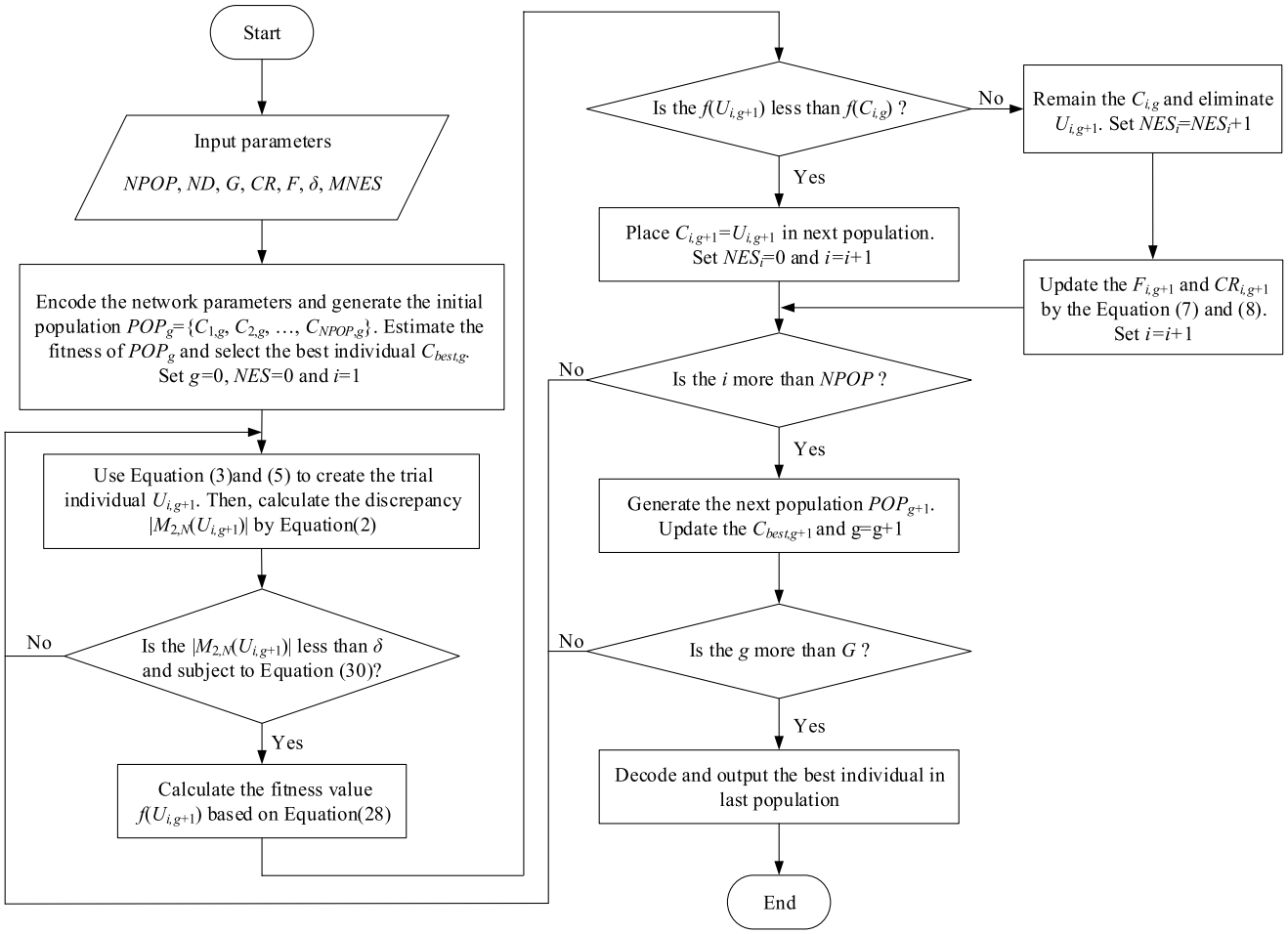


**FIGURE 6.** The procedure of NDMCDE for optimizing the network parameters.

force $F^U$ is obtained by bringing the variable $P_j^D$, $\theta$, $w$, $n^D$, $h$, $b$ and $\gamma^{D'}$ into Equation (13). The lift force $F^D$ is calculated by force equilibrium equation. Using variables $P_j^U$, $\theta$, $w$, $n^U$, $h$, $d$, $b$ and $F^D$, the $\gamma^U$ can be calculated by Equation (14). Subsequently, the variables $P_j^U$, $P_j^D$, $d$, $b$, $\theta$ as the input variables and the $\gamma^U$ as the target variable are selected to train the $M^U(*)$. Finally, the estimated value $\gamma^{U'}$ can be obtained based on the built prediction model $M^U(*)$.

## V. SERIAL HYBRID SOFT SENSOR MODEL

### A. FRAMEWORK OF SERIAL HYBRID SOFT SENSOR MODEL

The framework of serial hybrid soft sensor model is shown in Figure 5.

In the serial hybrid soft sensor model, two data driven models are connected before the derived mechanism model in serial way. The low discrepancy heuristic evolution extreme learning machine (LDHEELM) is proposed as the data driven model to estimate the jet impinging angles, $\gamma^{D'}$ and $\gamma^{U'}$. The prediction value of strip floating height $h'$ can be obtained by mechanism model according to the floating process data and the estimated $\gamma^{D'}$ and $\gamma^{U'}$.

The serial hybrid soft sensor model mainly consists of three phases: 1) Initialization phase. 2) Parameter estimation phase. 3) Floating height prediction phase. In the initialization phase, the floating process data is collected from the actual working conditions. In the parameter estimation phase, The $\gamma^{D'}$ is estimated by inputting the variables $P_j^U$, $P_j^D$, $\theta$ and $b$ into the model $M^D(*)$, while the value of $\gamma^{U'}$ is also estimated by the model $M^U(*)$ according to the variables $P_j^U$, $P_j^D$, $d$, $b$ and $\theta$. In the floating height prediction phase, based on the variables $P_j^U$, $P_j^D$, $\theta$, $w$, $d$, $b$ from the floating process data and the estimated $\gamma^{D'}$ and $\gamma^{U'}$, the prediction value of the strip floating height $h'$ is calculated by the derived mechanism model.

### B. LOW DISCREPANCY HEURISTIC EVOLUTION EXTREME LEARNING MACHINE

In this subsection, the LDHEELM is proposed. Different from the traditional ELM, the weights and bias of hidden layer in LDHEELM are assigned by LDSs method, which can guarantees the universal approximation property of the algorithm. Furthermore, a novel dual mutation strategy collaboration differential evolution algorithm (NDMCDE) is

proposed to optimize the performance of LDHEELM. The NDMCDE can avoid the destruction of the low discrepancy of the weights and bias in hidden layer.

In order to further improve the universal approximation property, the discrepancy is introduced into the fitness function. The fitness function is shown in Equation (28).

$$Minimize : f\left(o_k\right) = \frac{1}{2}\sum_{k=1}^{K}\left\|h_k - h'_k\right\|^2 + P\left(S\right) \tag{28}$$

where $h_k$ is the actual floating height at the $k$th sample. $h'_k$ is the floating height prediction value of serial hybrid soft sensor model at the $k$th sample. $S$ is a point set which composed of network parameters. $P(S)$ is the penalty function of the discrepancy and expressed as:

$$P\left(S\right) = \begin{cases} \left|M_{2,N}\left(S\right)\right| & if \left|M_{2,N}\left(S\right)\right| \le \xi \\ R & otherwise \end{cases} \tag{29}$$

where $R$ is the penalty value. $\xi$ is the threshold.

In addition, some researches show that adding physical constraints in training process can improve the generalization performance of the neural network algorithm [39], [40]. In air cushion furnace, the size of lower impinging angle slowly increases with the pressure of lower air boxes increases. The expression of inequality constraint can be derived by solving partial derivative of the $\gamma^{D'}$ with respect to input variable $P_j^D$ from Equation (1) and is represented by

$$\frac{\partial \gamma^{D'}}{\partial P_j^D} = \sum_{i=1}^{L}\beta_i H_i\left(1 - H_i\right)a_{2,i} > 0 \tag{30}$$

The procedure of NDMCDE for optimizing the network parameters is shown in Figure 6.

In the parameters optimization process, first, the initial population is created by encoding the network parameters. Subsequently, the trial individuals are created based on Equation (3) and (5). To avoid uniformity of parameters from being destroyed, the discrepancy is detected. The trial individuals whose discrepancy is less than $\delta$ are regarded as superior trial individuals; otherwise they are regarded as inferior trial individuals. If the trial individual is inferior, it will be replaced with new trial individual that is recreated by Equation (3) and (5). Then, the fitness of individuals is calculated by Equation (28). And the selection strategy is tournament method. Based on the fitness of individuals, the next population can be generated using the Equation (6). Meanwhile, the $F$ and $CR$ are updated based on the Equation (7) and (8) to promote the generation of new offspring. When the termination condition is satisfied, the optimal solution will be obtained by decoding the best individual in last population.

## VI. EXPERIMENT AND ANALYSIS

### A. PRESSURE TEST DEVICE

The pressure test device is independently designed and manufactured. In addition, the experiments are carried out on the pressure test device to obtain the pressure test data. The physical diagram of pressure test device is shown in Figure 7.

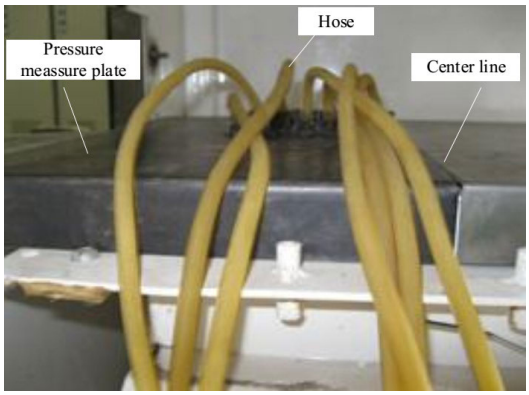


(a)

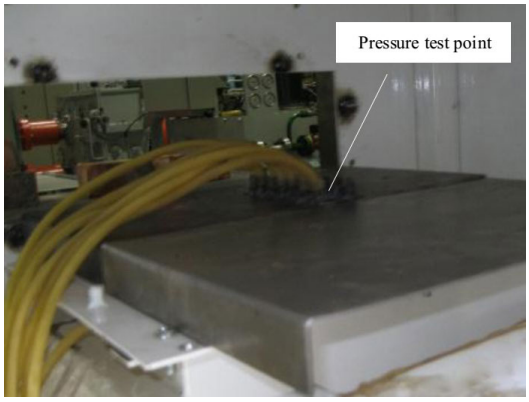


(b)

**FIGURE 7.** The physical diagram of pressure test device. (a) front view; (b) oblique view.

In the Figure 7, the pressure test device is comprised of lower air box, pressure measure plate, hoses and pressure sensors. The pressure measure plate is placed above the lower air box. The center line of the pressure measure plate coincides with the center line of the lower air box. The 7 pressure test points are installed on the left of center line of the pressure measure plate. In addition, the pressure sensors and the pressure test points are linked through yellow hoses.

In the experiments, the air flows impinge on the lower surface of pressure measure plate when the lower fan is working. Subsequently, the cushion pressure $P_c$ is obtained by the sensor with the change of the lower pressure $P_j^D$ and the height of pressure measure plate. Finally, the pressure test data can be obtained.

### B. INTRODUCTION OF EXPERIMENT EQUIPMENT

The proposed serial hybrid soft sensor model is verified on the self-development air cushion experiment platform. The structural diagram of platform is shown in Figure 8(a). The physical diagram of platform is shown in Figure 8(b). The air cushion experiment platform mainly consists of furnace body, upper air container, lower air container, upper fan, lower fan, slot nozzles, and air-seal devices. The size of platform is 3 m × 3 m × 2.2 m. The SIEMENS MM440 inverter is used to control the platform working. The laser range finder

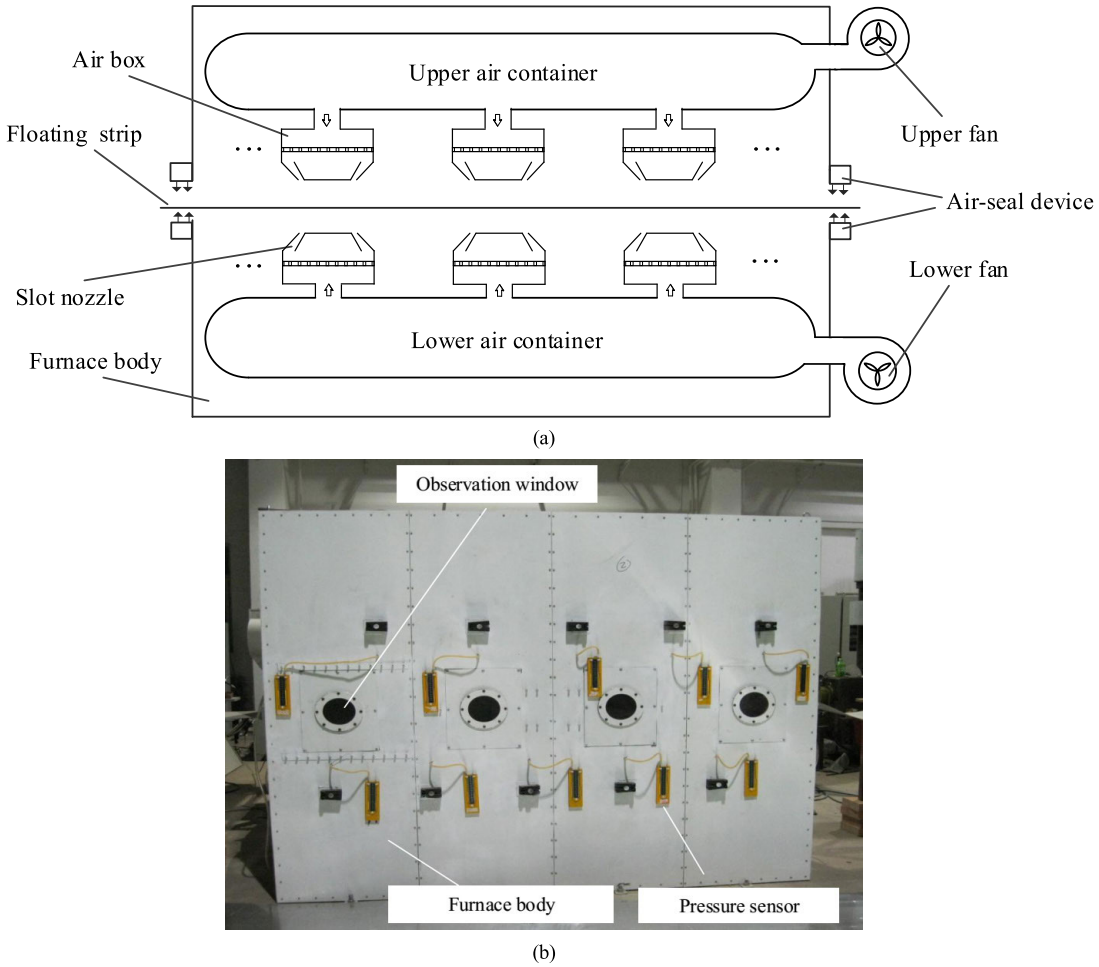


**FIGURE 8.** The physical diagram of the air cushion experiment platform. (a) the structural diagram of platform; (b) the physical diagram of platform.

is LOD2-250W150 and the resolution is 75 $\mu$m. The width of aluminum strip is 300 mm. The thickness of aluminum strip is 1.5 mm and 2 mm. The pressure of the nozzles is determined by the speed of the fans. The speeds of the upper and lower fans are controlled separately by the frequency converters.

During the operation process of the air cushion furnace, it took about 25 days to collect 1650 samples under the four specified working conditions in stable state. Among them, 26 samples are used to verify the effectiveness of the proposed model.

### C. EVALUATION STANDARD

The root mean square error (RMSE) and the mean absolute error (MAE) are scoring rules. Low RMSE and MAE indicate that the model has excellent predictive precision. In this paper, the RMSE and MAE as evaluation standard will be employed to measure the performance of proposed serial hybrid soft sensor model. The formulas of RMSE and MAE are shown in Equation (31) and (32).

$$RMSE = \sqrt{\frac{1}{K}\sum_{i=1}^{K}\left(y_i - y_i'\right)^2} \tag{31}$$

$$MAE = \frac{1}{K}\sum_{i=1}^{K}\left|y_i - y_i'\right| \tag{32}$$

where $K$ is the number of samples, $y_i$ is the actual value of $i$th sample, $y_i'$ is the prediction value of $i$th sample.

### D. RESULTS AND ANALYSIS

In our experiment, the pressures of upper air box were fixed at 70 Pa and 150 Pa. The floating heights of strips with two thicknesses of 1.5 mm and 2 mm were measured under different pressures of lower air box. The 6 independent experiments were performed on the experiment platform, and the average of the 6 prediction results was used as the final experiment result.

The prediction accuracy of the proposed serial hybrid soft sensor model (SHSSM) was compared with the bagging ensemble model of CART (BEMC), extreme learning machine model (ELM) and mechanism model (MM). In this experiment, the values of parameters are set as follow: $NPOP = 30, G = 100, F = 0.6, CR = 0.3$, Size($SP$)/Size($IP$) $= 1, MSPE = 3$. Furthermore,

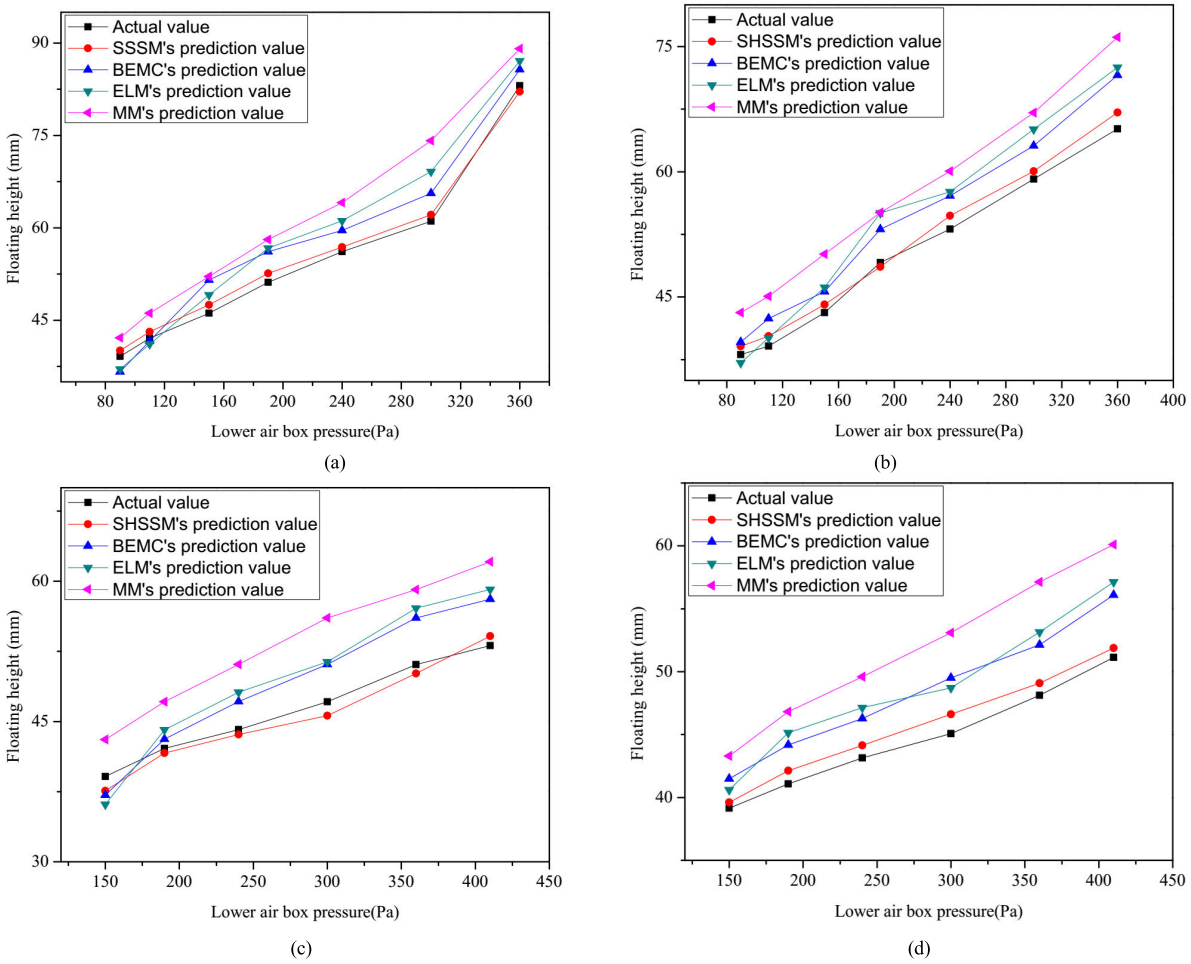


**FIGURE 9.** The diagram of prediction results and actual floating height. (a) thickness = 1.5 mm, upper pressure = 70 Pa; (b) thickness = 1.5 mm, upper pressure = 150 Pa; (c) thickness = 2 mm, upper pressure = 70 Pa; (d) Thickness = 2 mm, upper pressure = 150 Pa.

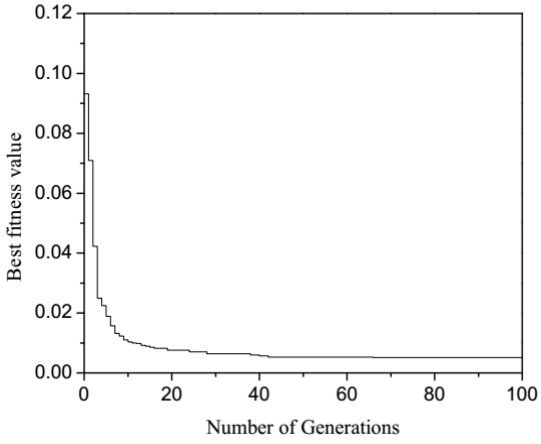


**FIGURE 10.** The diagram of best fitness value population for each generation.

the best hyper-parameters and the best network structure are determined through grid searching with cross-validation.

All the algorithms are implemented in a PC with Intel Core i7 CPU (3.80 GHz) and 32GB RAM. The experiment results of strip floating height are shown in Figure 9. Moreover, the best fitness value of the population for each generation is recorded in Figure 10.

In order to compare the prediction effect of proposed method with others three models clearly, the RMSE and MAE of prediction results are shown in Table 1 and Table 2. The minimums of RMSE and MAE are bold font under different work condition.

It can be seen from Table 1 and Table 2, the total RMSE and MAE of SHSSM are 4.4561 and 4.2169. The RMSE and the MAE of the BEMC are 15.1343 and 14.0856 respectively.

The RMSE and MAE of the ELM are 18.097 and 16.4409. The total RMSE and MAE of the MM are 29.2219 and 27.8715.

The performance of SHSSM is the best among four algorithms. The reason may be, for one thing, the proposed SHSSM combined the strong generalization ability of mechanism model and the strong learning ability of data driven model. For another, the mechanism model more comprehensively considered the influence factors of floating height and the performance of data driven model was improved by introducing the physical constraint and the indicator of discrepancy. The RMSE and MAE of BEMC and ELM are

**TABLE 1.** The RMSE values of different algorithms.

| | Strip Thickness = 1.5 mm | | Strip Thickness = 2 mm | | |
|---|---|---|---|---|---|
| Pressure (Pa) | 70 Pa | 150 Pa | 70 Pa | 150 Pa | Total |
| MM | 7.3585 | 7.3497 | 7.2357 | 7.278 | 29.2219 |
| ELM | 4.6429 | 4.7291 | 4.4596 | 4.2654 | 18.097 |
| BEMC | 3.7812 | 3.9391 | 3.6385 | 3.7755 | 15.1343 |
| SHSSM | **1.1108** | **1.2433** | **1.0842** | **1.0178** | **4.4561** |

**TABLE 2.** The MAE values of different algorithms.

| | Strip Thickness = 1.5 mm | | Strip Thickness = 2 mm | | |
|---|---|---|---|---|---|
| Pressure (Pa) | 70 Pa | 150 Pa | 70 Pa | 150 Pa | Total |
| MM | 6.7102 | 7.1262 | 6.9772 | 7.0579 | 27.8715 |
| ELM | 4.0899 | 4.1101 | 4.2089 | 4.032 | 16.4409 |
| BEMC | 3.4245 | 3.6717 | 3.3208 | 3.6686 | 14.0856 |
| SHSSM | **1.0866** | **1.162** | **1.0038** | **0.9645** | **4.2169** |

both larger than the SHSSM. The main reasons may be that the pure data driven model does not fully integrate the strong generalization of the mechanism model. The performance of BEMC is better than ELM. The reason may be that the BEMC is a strong learner and the ELM is single learner. The performance of ensemble model is better than single model. The performance of ELM is better than MM, the reason may be the size of jet impinging angles is set in MM by means of artificial experience, which has greater uncertainty and reduces the calculation accuracy of the model.

## VII. CONCLUSION

The high-quality metal strips play an important role in the national economic construction. The floating height has directly influence on the product quality and production efficiency of the strip. In order to achieve the accurate prediction of the floating height in air cushion furnace, a low discrepancy heuristic evolution ELM and ground effect theory based serial hybrid soft sensor model was proposed in this paper. Based on the ground effect theory and force equilibrium equation, the mechanism model was constructed, which reveals the mapping relationship between floating height and process variables. Subsequently, the two LDHEELM models were established to effectively estimate the lower and the upper jet impinging angles in the mechanism model. Furthermore, in order to guarantee the low discrepancy and physical applicability of data driven model, LDHEELM was improved by proposed NDMCDE. The experimental results showed that the SHSSM gets higher accuracy than BEMC, ELM and MM on the self-developed air cushion experiment platform. The proposed serial hybrid modeling method has certain reference value for the theoretical study of air cushion furnace. In addition, the research contents of this paper have practical significance for guaranteeing the surface quality and production efficiency of high-quality metal strips.

## REFERENCES


[1] V. K. Barnwal, S. Chakrabarty, A. Tewari, K. Narasimhan, and S. K. Mishra, "Forming behavior and microstructural evolution during single point incremental forming process of AA-6061 aluminum alloy sheet," *Int. J. Adv. Manuf. Technol.*, vol. 95, nos. 1–4, pp. 921–935, Mar. 2018.

[2] H. Shuai, W. Xiao, H. Fu-An, and W. Guo-Dong, "Research and development of the test platform for large air flotation type annealing furnaces," *J. Northeastern Univ.*, vol. 16, no. 2, p. 66, 2015.

[3] L. Yong, Z. Wang, M. Ma, G. Wang, T. Fu, and J. Li, "Review and prospect of the air cushion furnace technology for aluminium alloy automotive sheet pre-treatment," *Eng. Sci.*, vol. 16, no. 1, pp. 16–24, 2014.

[4] C. Wenxiu and D. Xiaoyou, "The analysis and experiment of plate-strip floating height in air cushion furnace," *J. Central South Univ.*, vol. 20, no. 8, pp. 251–259, 1989.

[5] P. M. Moretti, "Lateral deflections of webs in air-flotation ovens," *J. Appl. Mech.*, vol. 71, no. 3, pp. 314–320, May 2004.

[6] Y. B. Chang and P. M. Moretti, "Aerodynamic characteristics of pressure-pad air bars," *J. Appl. Mech.*, vol. 67, no. 1, pp. 177–182, Mar. 2000.

[7] L. I. Lu-Lei, C. Zhong-Qing, H. Sheng, and X. Pei-Min, "The equilibrium analysis of coupling system between axially moving paper and air cushion," *Mech. Res. Appl.*, vol. 26, no. 4, pp. 17–22, 2013.

[8] P. Zhou, P. Dai, H. Song, and T. Chai, "Data-driven recursive subspace identification based online modelling for prediction and control of molten iron quality in blast furnace ironmaking," *IET Control Theory Appl.*, vol. 11, no. 14, pp. 2343–2351, Sep. 2017.

[9] Y. Chen, K. Cai, Z. Tu, W. Nie, T. Ji, B. Hu, C. Chen, and S. Jiang, "Prediction of benzo [a] pyrene content of smoked sausage using back-propagation artificial neural network," *J. Sci. Food Agricult.*, vol. 98, pp. 3022–3030, Feb. 2018.

[10] W. Yan, D. Tang, and Y. Lin, "A data-driven soft sensor modeling method based on deep learning and its application," *IEEE Trans. Ind. Electron.*, vol. 64, no. 5, pp. 4237–4245, May 2017.

[11] X. Yuan, L. Li, Y. Shardt, Y. Wang, and C. Yang, "Deep learning with spatiotemporal attention-based LSTM for industrial soft sensor model development," *IEEE Trans. Ind. Electron.*, early access, Apr. 9, 2020, doi: 10.1109/TIE.2020.2984443.

[12] Y. Wu, D. Liu, X. Yuan, and Y. Wang, "A just-in-time fine-tuning framework for deep learning of SAE in adaptive data-driven modeling of time-varying industrial processes," *IEEE Sensors J.*, vol. 21, no. 3, pp. 3497–3505, Feb. 2020.

[13] X. Yuan, C. Ou, Y. Wang, C. Yang, and W. Gui, "A layer-wise data augmentation strategy for deep learning networks and its soft sensor application in an industrial hydrocracking process," *IEEE Trans. Neural Netw. Learn. Syst.*, early access, Dec. 13, 2019, doi: 10.1109/TNNLS.2019.2951708.

[14] G.-B. Huang, Q.-Y. Zhu, and C.-K. Siew, "Extreme learning machine: A new learning scheme of feedforward neural networks," in *Proc. IEEE Int. Joint Conf. Neural Netw.*, vol. 2, Jul. 2004, pp. 985–990.

[15] W. Sun, C. Wang, and C. Zhang, "Factor analysis and forecasting of $CO_2$ emissions in Hebei, using extreme learning machine based on particle swarm optimization," *J. Cleaner Prod.*, vol. 162, pp. 1095–1101, Sep. 2017.

[16] C. Wei, K. Fanbei, W. Baoxiang, and L. Yuhan, "Application of grey relational analysis and extreme learning machine method for predicting silicon content of molten iron in blast furnace," *Ironmaking Steelmaking*, vol. 46, no. 10, pp. 974–979, 2018.

[17] C. Cervellera and D. Maccio, "Low-discrepancy points for deterministic assignment of hidden weights in extreme learning machines," *IEEE Trans. Neural Netw. Learn. Syst.*, vol. 27, no. 4, pp. 891–896, Apr. 2016.

[18] Y. Zhou, N. Zhou, L. Gong, and M. Jiang, "Prediction of photovoltaic power output based on similar day analysis, genetic algorithm and extreme learning machine," *Energy*, vol. 204, Aug. 2020, Art. no. 117894.
[19] Y. Li and H. Hu, "Influential factor analysis and projection of industrial $CO_2$ emissions in China based on extreme learning machine improved by genetic algorithm," *Polish J. Environ. Stud.*, vol. 29, no. 3, pp. 2259–2271, 2020.
[20] D. Wu, Z. S. Qu, F. J. Guo, X. L. Zhu, and Q. Wan, "Hybrid intelligent deep kernel incremental extreme learning machine based on differential evolution and multiple population grey wolf optimization methods," *Automatika*, vol. 60, no. 1, pp. 48–57, Jan. 2019.
[21] W. Guo, T. Xu, and Z. Lu, "An integrated chaotic time series prediction model based on efficient extreme learning machine and differential evolution," *Neural Comput. Appl.*, vol. 27, no. 4, pp. 883–898, May 2016.
[22] J. Cao, Z. Lin, and G.-B. Huang, "Self-adaptive evolutionary extreme learning machine," *Neural Process. Lett.*, vol. 36, no. 3, pp. 285–305, Dec. 2012.
[23] Y. Li, S. Wang, and B. Yang, "An improved differential evolution algorithm with dual mutation strategies collaboration," *Expert Syst. Appl.*, vol. 153, Sep. 2020, Art. no. 113451.
[24] C. Wang, J. Xu, Y. Chen, L. Bai, and Z. Chen, "A hybrid model to assess the impact of climate variability on streamflow for an ungauged mountainous basin," *Climate Dyn.*, vol. 50, nos. 7–8, pp. 2829–2844, Apr. 2018.
[25] Y. Liu, C.-P. Chou, J. Chen, and J.-Y. Lai, "Active learning assisted strategy of constructing hybrid models in repetitive operations of membrane filtration processes: Using case of mixture of bentonite clay and sodium alginate," *J. Membrane Sci.*, vol. 515, pp. 245–257, Oct. 2016.
[26] J. A. Barrios, C. Villanueva, A. Cavazos, and R. Colás, "Fuzzy C-means rule generation for fuzzy entry temperature prediction in a hot strip mill," *J. Iron Steel Res. Int.*, vol. 23, no. 2, pp. 116–123, Feb. 2016.
[27] J. Wei and X. Gao, "Electric-parameter-based inversion of dynamometer card using hybrid modeling for beam pumping system," *Math. Problems Eng.*, vol. 2018, pp. 1–12, Jun. 2018.
[28] X. Wang and H. Liu, "A Knowledge- and data-driven soft sensor based on deep learning for predicting the deformation of an air preheater rotor," *IEEE Access*, vol. 7, pp. 159651–159660, 2019.
[29] S. Hou, F. Hua, W. Lv, Z. Wang, Y. Liu, and G. Wang, "Hybrid modeling of flotation height in air flotation oven based on selective bagging ensemble method," *Math. Problems Eng.*, vol. 2013, pp. 1–9, Jan. 2013.
[30] S. Hou, J. Liu, and W. Lv, "Flotation height prediction under stable and vibration states in air cushion furnace based on hard division method," *Math. Problems Eng.*, vol. 2019, pp. 1–14, Dec. 2019.
[31] S. Hou, X. Zhang, W. Dai, X. Han, and F. Hua, "Multi-model- and soft-transition-based height soft sensor for an air cushion furnace," *Sensors*, vol. 20, no. 3, p. 926, Feb. 2020.
[32] J. Zhang, Z.-Z. Mao, R.-D. Jia, and D.-K. He, "Serial hybrid modelling for a gold cyanidation leaching plant," *Can. J. Chem. Eng.*, vol. 93, no. 9, pp. 1624–1634, Sep. 2015.
[33] W. Lv, Z. Xie, Z. Mao, P. Yuan, and M. Jia, "Hybrid modelling for real-time prediction of the sulphur content during ladle furnace steel refining with embedding prior knowledge," *Neural Comput. Appl.*, vol. 25, no. 5, pp. 1125–1136, Oct. 2014.
[34] A. Georgieva and I. Jordanov, "Global optimization based on novel heuristics, low-discrepancy sequences and genetic algorithms," *Eur. J. Oper. Res.*, vol. 196, no. 2, pp. 413–422, Jul. 2009.
[35] W. J. Morokoff and R. E. Caflisch, "Quasi-random sequences and their discrepancies," *SIAM J. Scientific Comput.*, vol. 15, no. 6, pp. 1251–1279, Nov. 1994.
[36] F. M. De Rainville, C. Gagne, O. Teytaud, and D. Laurendeau, "Evolutionary optimization of low-discrepancy sequences," *ACM Trans. Model. Comput. Simul.*, vol. 22, no. 2, p. 25, Mar. 2012, Art. no. 9.
[37] R. Storn and K. Price, "Differential evolution-a simple and efficient heuristic for global optimization over continuous spaces," *J. Global Optim.*, vol. 11, no. 4, pp. 341–359, 1997.
[38] L. Deng, H. Sun, and C. Li, "JDF-DE: A differential evolution with Jrand number decreasing mechanism and feedback guide technique for global numerical optimization," *Appl. Intell.*, vol. 51, no. 1, pp. 359–376, Jan. 2021.
[39] S. Milanič, S. Strmčnik, D. Šel, N. Hvala, and R. Karba, "Incorporating prior knowledge into artificial neural networks—An industrial case study," *Neurocomputing*, vol. 62, pp. 131–151, Dec. 2004.
[40] Y. Zhang, S. Li, S. Kadry, and B. Liao, "Recurrent neural network for kinematic control of redundant manipulators with periodic input disturbance and physical constraints," *IEEE Trans. Cybern.*, vol. 49, no. 12, pp. 4194–4205, Dec. 2019.

**SHUAI HOU** received the M.Sc. and Ph.D. degrees from Northeastern University, China, in 2009 and 2015, respectively. He is currently an Associate Professor with the Hebei University of Engineering, China. During his Ph.D. period, he was mainly engaged in the research of air cushion furnace and equipment development. His current research interests include intelligent manufacturing and machine learning. In addition, he specializes in the study combination of industrial process control and artificial intelligence (AI).

**JITONG LIU** is currently pursuing the master's degree with the School of Information and Electrical Engineering, Hebei University of Engineering. His research interest includes machine learning. His main research direction includes the study of combination industrial process control with intelligent algorithms.

**MEIJUAN BAI** received the master's degree in circuits and systems from the Taiyuan University of Science and Technology, Taiyuan, China, in 2016. She is currently an Assistant Experimenter of Communication Engineering with the Hebei University of Engineering, Handan, China. Her research interests include image processing, pattern recognition, and machine learning.

**FUAN HUA** received the Ph.D. degree in materials processing engineering from the Institute of Metal Research, Chinese Academy of Sciences, Shenyang, China, in 2004. He is currently a Professor of Materials Processing Engineering with Northeastern University, Shenyang. His research interests include material processing, modeling and simulation of material processing, development of material processing equipment, and machine learning application in materials science.

**XIAOLIN HAN** is currently pursuing the master's degree with the School of Information and Electrical Engineering, Hebei University of Engineering. Her research interest includes machine learning. Her main research direction includes the study of combination industrial process control with machine learning.

**WEIWEI LIU** received the Ph.D. degree in mechanical engineering from Northeastern University, Shenyang, China, in 2009. He is currently an Associate Professor of Mechanical Engineering with the Dalian University of Technology, Dalian, China. His research interests include intelligent manufacturing, green manufacturing, laser additive manufacturing, computer vision, and intelligent control.